EARTHQUAKE ENGINEERING AND STRUCTURAL DYNAMICS, VOL. 24, 491–503 (1995)

OBSERVATION AND NUMERICAL ANALYSIS OF SOIL–STRUCTURE INTERACTION OF A REINFORCED CONCRETE TOWER

TODOR GANEV*, FUMIO YAMAZAKI† AND TSUNEO KATAYAMA‡
Institute of Industrial Science, The University of Tokyo, 7-22-1, Roppongi, Minato-ku, Tokyo 106, Japan

SUMMARY

A vast amount of earthquake response records of an observation tower are used together with microtremor data to investigate various aspects of the dynamic behaviour of the soil–structure system. It is found that separation of the soil from the structure occurs under large dynamic loads, leading to changes in the predominant frequency of the system. As a result of the decreasing of the soil support at the side walls of the foundation, the stress caused by the structural weight on the bottom soil increases during earthquakes. With regard to its practical applicability, a linear sway-rocking model is applied for numerical modelling of the soil–structure system. Alterations in the soil support as a result of soil non-linearity and separation of the structure from the soil are investigated by comparing recorded and simulated structural response. The influence of each of these factors on the softening of the soil support is distinctly assessed. An empirical relationship between the peak ground velocity and the soil constants for earthquake excitations of different magnitude is presented.

INTRODUCTION

Considering the interaction between soil and structure is important especially for the design of large structures with embedment such as, for instance, nuclear power plant buildings and foundations of suspension bridges. Many sophisticated analytical and numerical approaches to the problem of dynamic soil–structure interaction have been developed in the past decades (e.g. References 1–5). At the same time, publicized data from observation of actual response of structures including free field motion and soil pressure are still relatively few. An example of the usefulness of such observations for evaluation of existing analysis practices is the large scale seismic experiment in Lotung, Taiwan.[6]

To provide verification data of soil–structure interaction, a model reinforced concrete tower has been constructed in the Chiba Experiment Station of the Institute of Industrial Science, University of Tokyo. The accelerometers and soil pressure gauges, installed in it, have been in operation since August 1983 and have provided records from more than 200 earthquakes. The motion of the free field near the structure has been thoroughly observed using the three-dimensional Chiba seismometer array.[7] Some aspects of the soil–structure interaction of the model tower have already been analysed by previous researchers.[8,9]

In the present study, a simple sway-rocking model, chosen with regard to its practical applicability, was applied to simulate the behaviour of the observation tower. The objective of this paper is to present results of analysis of earthquake and microtremor data as well as values of parameters of the soil–structure system, determined by observation and numerical modelling.

*Graduate student.
†Associate Professor.
‡Professor.

CCC 0098–8847/95/040491–13

Received 14 April 1993
Revised 8 July 1994

DESCRIPTION OF THE TOWER AND THE OBSERVATION SYSTEM

The Chiba Experiment Station is located about 30 km east of Tokyo, at a geographical longitude of 140° 6′ 37″ E and a latitude of 35° 37′ 17″ N. A view of the observation tower is shown in Figure 1. It is constructed at an approximate distance of 15 m from borehole P5 of the Chiba seismometer array.[7] The structure consists of four floors and a basement, with a total height of 10 m above the ground level and 2·5 m underground (Figure 2). Its cross-section is a regular octagon. The thickness of the walls is 180 mm above the ground level and 500 mm in the basement. The thickness of all the floor slabs is 150 mm, with the exception of the basement floor slab, which is 500 mm. The slab of the second floor has an octagonal opening in the middle. The foundation lies on sand layer of thickness 100 mm. Thirteen accelerometers are attached to the floor slabs of the tower, including the basement floor. Twenty-five soil pressure gauges are installed at contact points between the basement of the tower and the surrounding soil, as shown in Figure 2. The same figure shows the positive directions in the local co-ordinate system (OXY), associated with the structure. The soil profile at borehole P5 is relatively simple with rather uniform layering.[7]

In the present study a large amount of earthquake data recorded during the past 10 years at the observation tower, were used. A representative list of some of the analysed earthquakes can be seen in Table I. The largest event included was the Chibaken-Toho-Oki Earthquake of 17 December 1987 (IEQK 8722). Its peak ground acceleration (PGA) of the North–South (NS) component recorded at ground level (GL) − 1 m at borehole P5 is 393 cm/s^2 and that of the OX-component is 305 cm/s^2. The earthquake response records of the tower were processed in a similar manner as the records of the Chiba Array Database.[7] The soil pressure gauges can measure only dynamic increments relative to an initial value, which depends on the

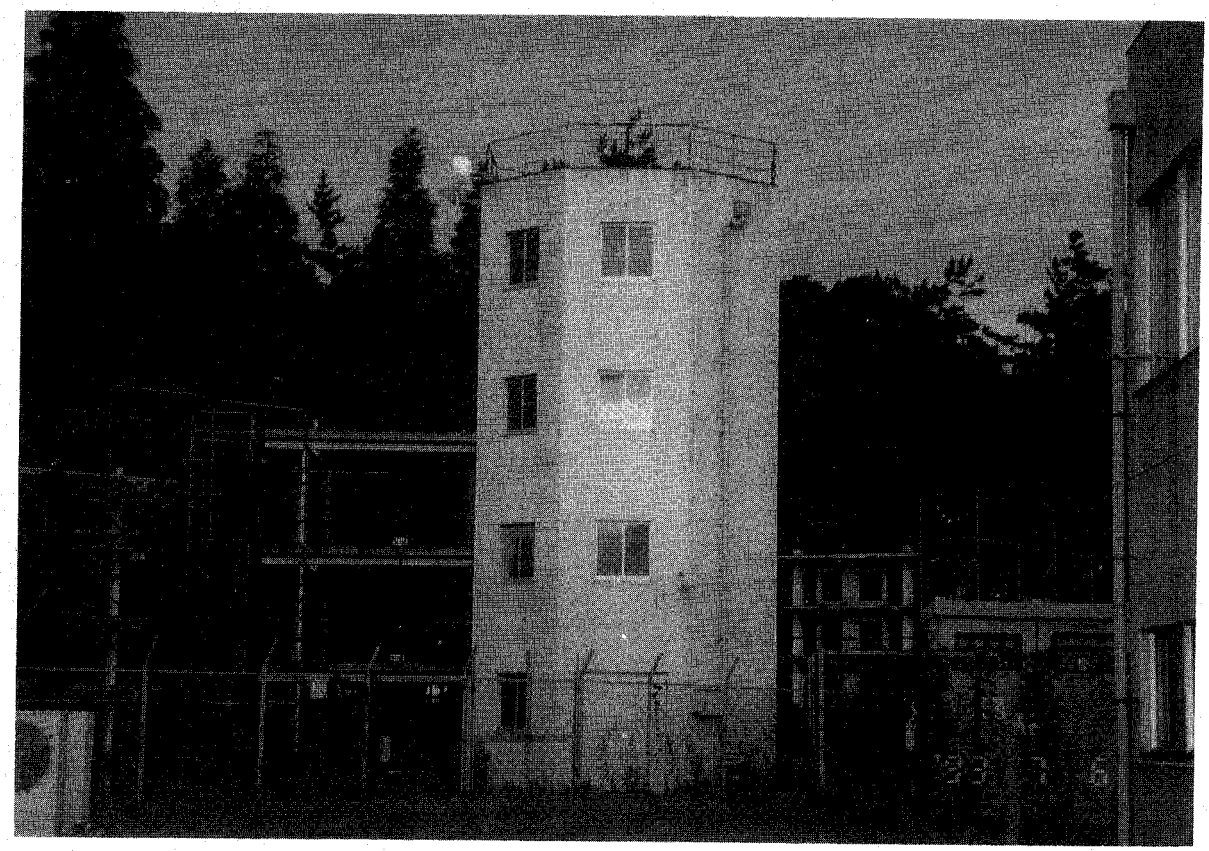

Figure 1. View of the observation tower

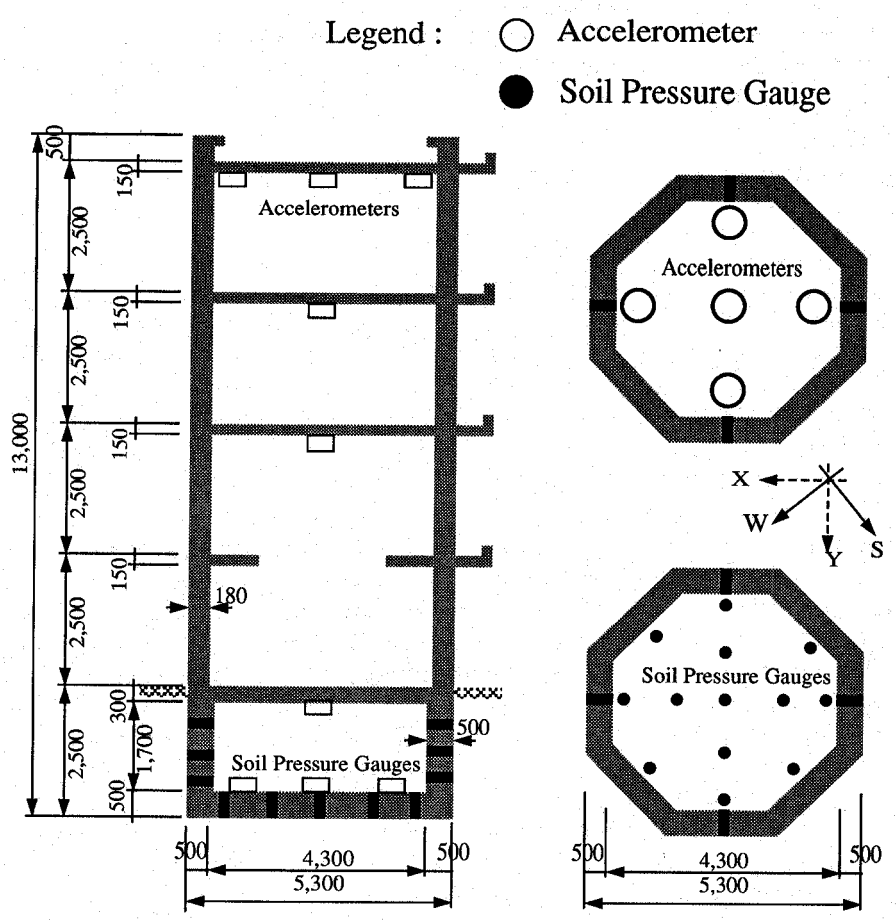

Figure 2. Vertical and horizontal cross-sections of the tower (dimensions in mm)

Table I. Summary of the earthquake events used in the analysis

No.	IEQK	Trigger time at P540 (Borehole P5, GL-40 m) Date	h/min/s	Max acceleration at P501 [cm/s^2] (Borehole P5, GL-1 m) OX	OY	OZ	Max acceleration at the tower roof [cm/s^2] OX	OY	OZ
1	8519	04-10-85	21:25:51	83·4	79·2	27·2	213·3	180·2	32·9
2	8525	06-11-85	00:31:00	73·8	76·0	29·2	153·9	193·0	41·6
3	8717	30-06-87	18:17:21	21·1	25·8	12·2	41·1	54·0	15·7
4	8722	17-12-87	11:08:27	304·9	277·1	121·9	761·0	677·1	139·0
5	8723	17-12-87	11:15:14	19·4	26·4	11·3	41·9	32·4	21·1
6	8726	17-12-87	15:30:07	21·6	37·8	18·7	19·1	41·0	20·0
7	8806	18-01-88	19:37:24	35·9	99·4	19·3	77·2	146·5	25·8
8	8816	18-03-88	05:34:45	52·4	59·4	41·8	184·1	110·1	38·7

starting time of each record. For this reason, the true dynamic soil pressure time histories were obtained by subtracting the initial values from all the records. A series of microtremor observations was conducted at daytime on 23 November 1992. Each observation was carried out using simultaneously three velocity-type sensors. They were placed at points of interest in 16 different configurations to enable evaluation of transfer

functions between the free field and the structure and between different parts of the structure. Since the pick-ups have flat sensitivity between 1 and 10 Hz, the frequency contents outside this range were eliminated by a cosine-type band-pass filter.

OBSERVATION OF SOIL–STRUCTURE INTERACTION EFFECTS

Shift of the predominant frequency of the soil–structure system

Figure 3 shows Fourier spectrum ratios between the free field acceleration (recorded at borehole P5, GL-1 m) and the response of the fourth floor of the tower. It can be seen that depending on the amplitude of the dynamic excitation, the behaviour of the soil–structure system significantly changes. There is a marked shift of the dominant frequency from about 4·0 Hz for the microtremor through 3·5 Hz for a moderate earthquake (IEQK 8519, PGA = 70 cm/s^2) to 2·5 Hz for the considerably larger Chibaken-Toho-Oki Earthquake (IEQK 8722, PGA = 393 cm/s^2). Each of the Fourier spectrum ratios between the free-field motion and the tower response has a single distinct peak. This shows the effect of kinematic interaction, which causes attenuation of the high frequency contents.[10] Considering the high rigidity of the structure, it can be surmised that the first predominant frequency corresponds to the rocking mode. To verify this, the horizontal displacements of each floor, which are caused only by rocking and not by the elastic structural response were extracted from the total response through a simple procedure. The vertical displacements at the floor of the foundation were evaluated by double integration of the acceleration time histories. The basement floor slab is very rigid and experiences almost no bending during earthquake. Therefore, by dividing the relative displacement of opposite points of the foundation plate by the distance between them and calculating the arc tangent of the ratio, the angle of rocking at each time step could be evaluated. Multiplying the rocking angle time history by the height of each floor of the structure, we obtained the corresponding horizontal displacements, which are due only to the rocking. The Fourier spectrum ratios between the free field acceleration and that, caused by the rocking had single distinct peaks at exactly the same frequencies, as the ones, calculated for the total response, which confirmed the above supposition.

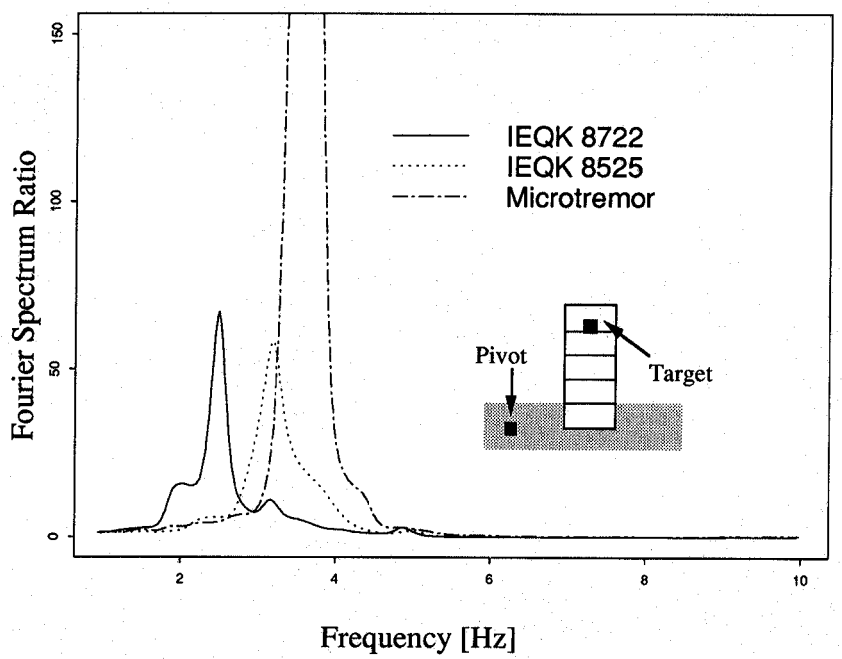

Figure 3. Fourier spectrum ratios between the soil and the fourth floor of the tower

Separation of the basemat and the side walls of the foundation from the soil

Figure 4 presents time histories of the dynamic parts of the soil pressure from the Ibarakiken-Nambu Earthquake (IEQK 8519), recorded at points, lying in the vertical plane XOZ (for the directions OX, OY and OZ see Figures 2 and 6). This moderate earthquake is used only here to provide a consistent overall illustration, since some of the soil pressure records of the Chiba-Toho-Oki Earthquake are unclear due to overscaling of the gauges. The drifts, exhibited by the records, show the inelastic and non-linear behaviour of the soil at the measuring points, resulting in unrecovered deformations, at least for the duration of the

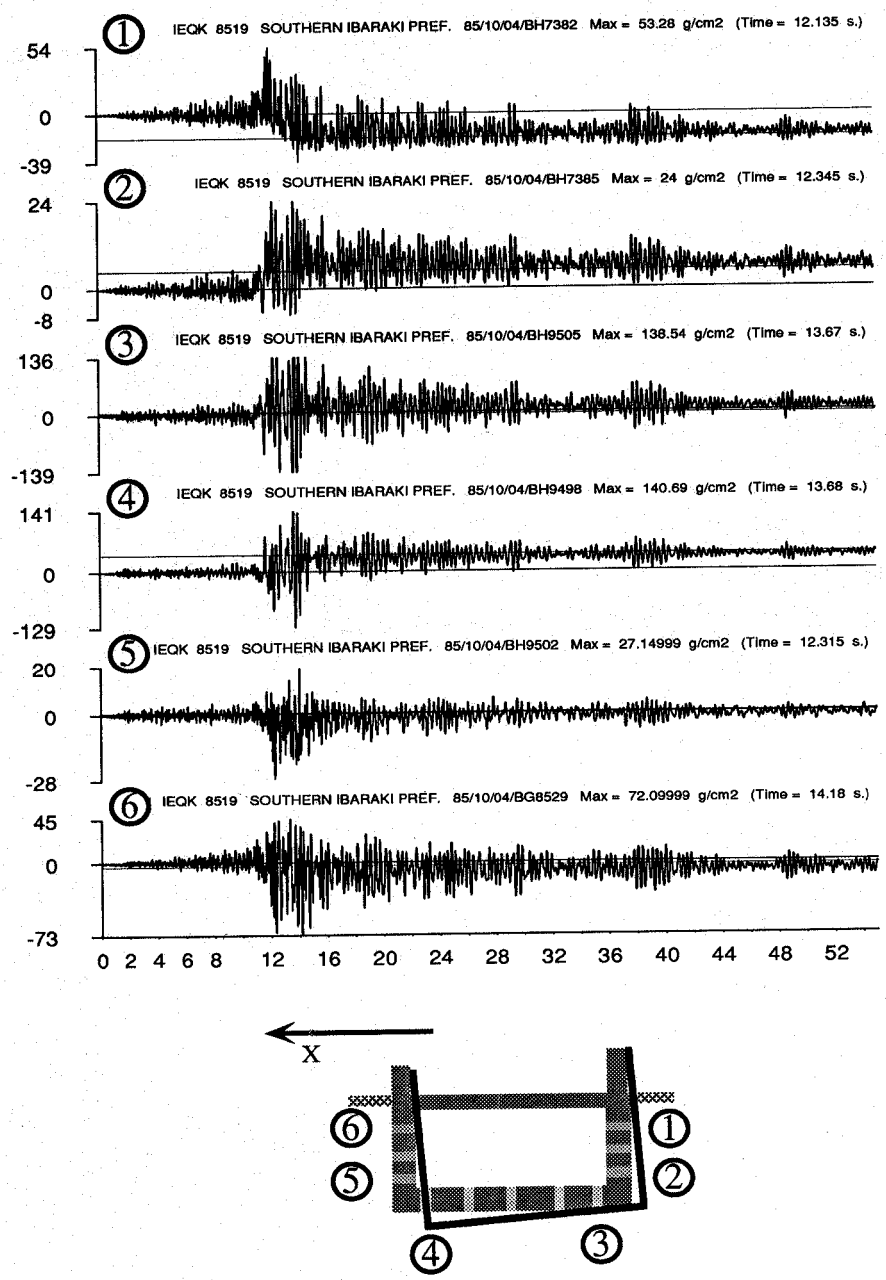

Figure 4. Time histories of soil pressure (IEQK 8519) (pressures in g/cm^2; 1 g/cm^2 = 98·07 N/m^2)

earthquake. Figure 4 shows also a qualitative evaluation of the new position of the tower, due to these deformations. This evaluation, however, should not be accepted without reserve, because the nature of the deformations is not certain. It is possible that the permanent displacements were only local effects, due to the penetration of the gauge itself into the soil. The time history of dynamic soil pressure, recorded by Gauge 1 (Figure 4) shows a shift of the baseline in the negative direction, i.e. a general decreasing of the contact pressure between soil and structure. As a large portion of the time history is asymmetrical, the position of the shifted baseline is determined on the basis of the symmetrical soil pressure values recorded at the end of the earthquake. In the period between 13 and 40 s the negative peaks attain almost equal values. With respect to the shifted baseline they are smaller in absolute value than the positive peaks and do not exceed a certain bound. This effect has been observed by previous researchers.[8] It suggests that the soil was separated from the side wall of the structure. Considering the separation, the significant increase of the bottom pressure can be explained as a result not only of rocking, but also of the redistribution of stresses from the structural weight when the side wall separates from the soil. Neither drifts nor separation were observed at small earthquakes, which shows that both phenomena are dependent on the intensity of the earthquake motion.

The absolute soil pressure time histories were obtained as the sum of the static and dynamic pressure at each point and were used to assess quantitatively the separation of the soil from the structure. The criterion for occurring of separation was the state, in which the absolute soil pressure becomes 0 or negative. The time instants, at which the absolute soil pressure becomes non-positive for each of the gauges were detected. Some examples of distributions of the absolute soil pressure at such frozen times are presented in Figure 5 for the Chibaken-Toho-oki Earthquake. The points at which non-positive values of the absolute soil pressure were detected are hatched in the perspective plot in Figure 6. Simultaneous separation at all those points during the Chibaken-Toho-Oki Earthquake (IEQK 8722) was observed, which means that at least about 12 per cent of the area of the walls (2 out of 12 gauges plus the area between them) and 20 per cent of the area of the bottom of the foundation (3 out of 13 gauges) did not participate in the support of the structure.

NUMERICAL MODELLING OF THE SOIL–STRUCTURE SYSTEM

The sway-rocking model shown in Figure 7 was chosen for numerical modelling of the observation tower. The motion of the system is represented by

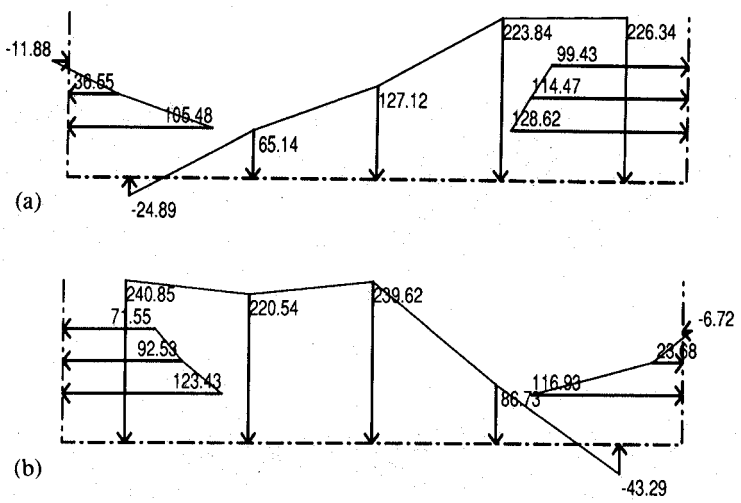

Figure 5. Absolute soil pressure distributions at frozen time moments (IEQK 8722) (pressures in g/cm^2; 1 g/cm^2 = 98·07 N/m^2): (a) plane OXZ (IEQK 8722 time = 9·525 s); (b) plane OYZ (IEQK 8722 Time = 10·000 s)

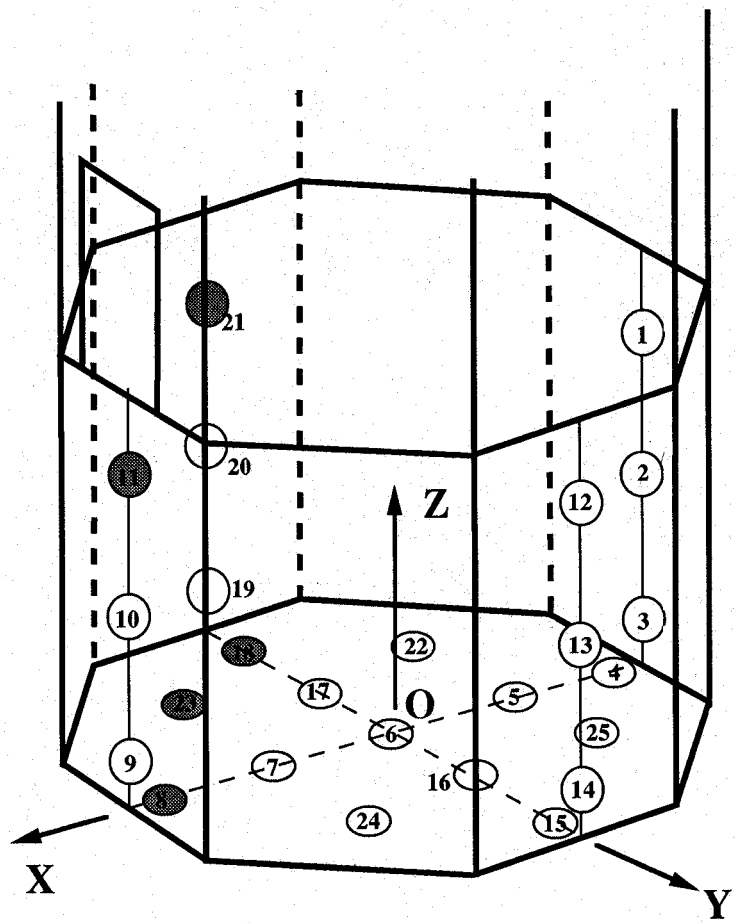

Figure 6. Locations at which separation of the structure from the soil during Event 8722 was detected

$$m_i(\ddot{y}_i + \ddot{z}_0) + \sum_{j=1}^{n} c_{ij}(\dot{y}_j - \dot{y}_0 - \dot{\theta}H_j) + \sum_{j=1}^{n} k_{ij}(y_j - y_0 - \theta H_j) = 0 \tag{1}$$

$$m_0(\ddot{y}_i + \ddot{z}_0) + C_H\dot{y}_0 + K_H y_0 - \sum_{i=1}^{n}\sum_{j=1}^{n} c_{ij}(\dot{y}_j - \dot{y}_0 - \dot{\theta}H_j) - \sum_{i=1}^{n}\sum_{j=1}^{n} k_{ij}(y_j - y_0 - \theta H_j) = 0 \tag{2}$$

$$I\ddot{\theta} + C_R\dot{\theta} + K_R\theta - \sum_{i=1}^{n}\sum_{j=1}^{n} c_{ij}H_i(\dot{y}_j - \dot{y}_0 - \dot{\theta}H_j) - \sum_{i=1}^{n}\sum_{j=1}^{n} k_{ij}H_i(y_j - y_0 - \theta H_j) = 0 \tag{3}$$

in which (Figure 7) K_R is the rocking spring constant, K_H is the sway spring constant, C_R is the rocking dashpot constant, C_H is the sway dashpot constant, m_i are concentrated masses, k_{ij} are the stiffness influence coefficients of the superstructure, c_{ij} are the damping influence coefficients of the superstructure, I is the mass moment of inertia of the superstructure about the centre of rocking, H_i are the heights of the concentrated masses, y_i is the displacement of the concentrated mass m_i relative to the displacement of the ground, θ is the angle of rocking and z_0 is the input motion. After determination of the input parameters as discussed below, the system of equation was solved by direct integration applying the Newmark β method.[11]

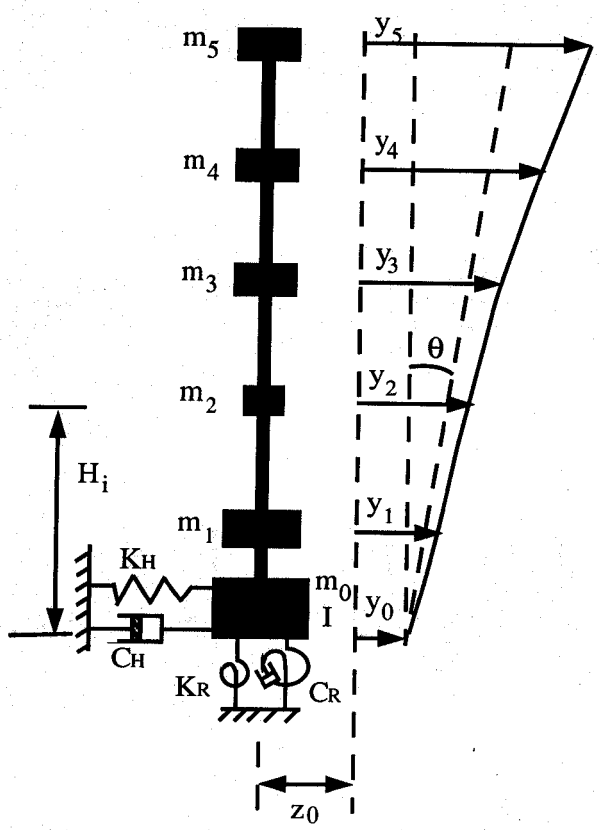

Figure 7. Modelling of the soil–structure system

Determination of the input motion

The input motion was specified in the form of effective motion, deconvolved from the free field motion by a procedure developed by Harada *et al.*[12] as

$$\frac{z_0'}{z_0} = \begin{cases} \left|\dfrac{\sin \zeta h}{\zeta h}\right|, & 0 \leqslant \zeta h \leqslant \pi/2 \\ 0{\cdot}63 & \zeta h \geqslant \pi/2 \end{cases} \tag{4}$$

in which z_0' is the effective motion, z_0 is the free-field motion and h is the depth of embedment. The coefficient ζ is evaluated as

$$\zeta = \frac{\omega}{V_s\sqrt{1 + \mathrm{i}2D}} \tag{5}$$

where D is the damping ratio of the soil, V_s is the shear wave velocity of the soil, ω is the circular frequency and $\mathrm{i} = \sqrt{-1}$.

Determination of the soil stiffness and damping coefficients

Appropriate constant values for the soil stiffness and damping coefficients were determined on the basis of the methodology proposed in Reference 12:

$$K_H = \kappa_1 Ga\left(b_{u1} + \frac{G_s}{G}\frac{h}{a}s_{u1}\right) \tag{6}$$

$$K_R = \kappa_2 Ga^3\left[b_{\psi 1} + \left(\frac{z_c}{a}\right)^2 b_{u1} + \frac{G_s}{G}\frac{h}{a}s_{\psi 1} + \frac{G_s}{G}\left(\frac{h^2}{3a^3} + \frac{hz_c^2}{a^3} - \frac{h^2 z_c}{a^3}\right)s_{u1}\right] \tag{7}$$

$$C_H = \kappa_3 \frac{Ga}{\omega}\left(b_{u2} + \frac{G_s}{G}\frac{h}{a}s_{u2}\right) \tag{8}$$

$$C_R = \kappa_4 \frac{Ga^3}{\omega}\left[b_{\psi 2} + \left(\frac{z_c}{a}\right)^2 b_{u2} + \frac{G_s}{G}\frac{h}{a}s_{\psi 2} + \frac{G_s}{G}\left(\frac{h^3}{3a^3} + \frac{hz_c^2}{a^3} - \frac{h^2 z_c}{a^3}\right)s_{u2}\right] \tag{9}$$

where G_s is the shear modulus of the surface stratum, G is the shear modulus of the soil under the foundation, z_c is the height of the center of gravity of the foundation, a is the radius of foundation, h is the depth of embedment and ω is the circular frequency. b_i are dimensionless dynamic stiffness functions for a flat foundation resting on the soil surface. s_i are dimensionless dynamic stiffness functions defined for unit depth of the surface stratum. b_i and s_i represent, respectively, the contribution of the soil at the bottom and around

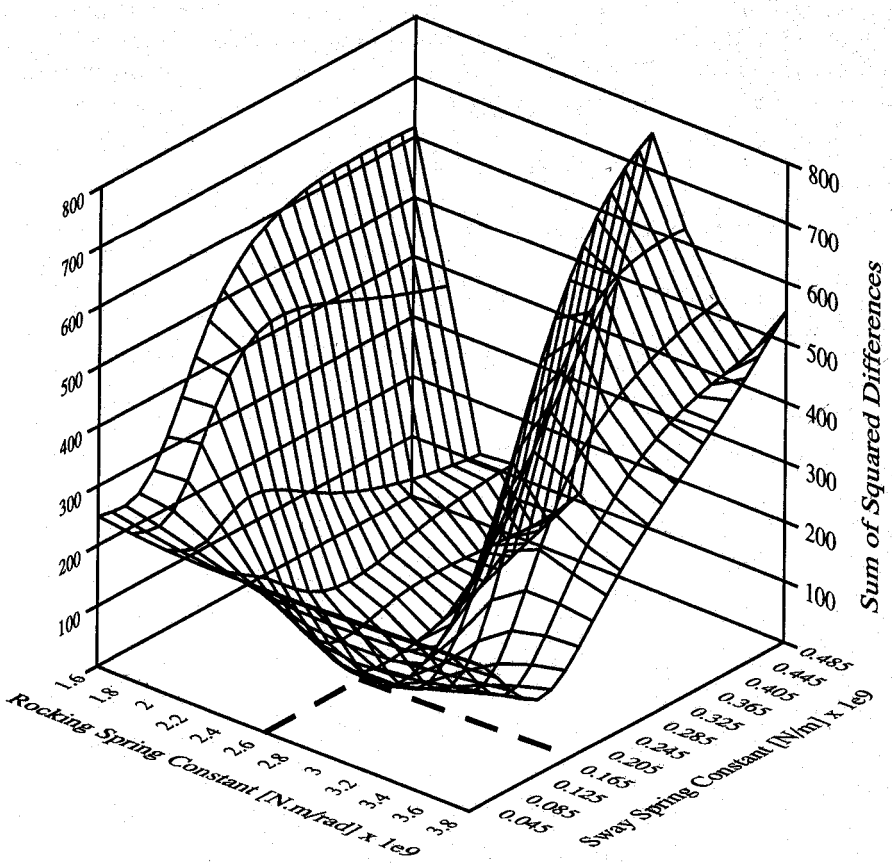

Figure 8. Determination of soil stiffness constants for the OX-component of Event 8722

the side walls of the foundation to the overall stiffness and damping. (The subscript u is associated with horizontal displacement and the subscript ψ, with rotation. They signify that the corresponding function expresses resistance of soil to the respective type of motion.) The evaluation of these functions is a heavy computational task. Details can be found in Reference 12. κ_i are softening coefficients, which were added by the present authors to account for separation effects and non-linearity.

Since during small earthquakes separation does not occur, the initial values for the coefficients were obtained by substituting $\kappa_1 = \kappa_2 = \kappa_3 = \kappa_4 = 1$ in equations (6)–(9). The static values of the stiffness coefficients (at $\omega = 0$ Hz) were used as the basis for analysis. The such selected constants produced good agreement with regard to the frequency contents of real and calculated response for small events (e.g. IEQK 8717, PGA = 24 cm/s^2). Appropriate values of the stiffness coefficients (respectively, κ_1 and κ_2) for larger earthquakes were found by trial and error. The squared sum of differences between the Fourier spectra of the real and calculated response in the range 2–6 Hz was used as a criterion for the best-fitting values of K_R and K_H (respectively, κ_1 and κ_2). Figure 8 shows an example of determination of the constants for one horizontal component of the Chibaken-Toho-Oki Earthquake. The squared sum of differences between the Fourier spectra of the real and calculated response is plotted as a function of the soil spring coefficients used in the multiple trial and error computations for this case. The best-fitting values of K_R and K_H are those, for which the function has a minimum. During this step of the analysis we were concerned with fitting the recorded response only in terms of its frequency contents, so we varied only the soil stiffness and the values of C_R and C_H were kept unchanged in all cases. Once the values of the stiffness coefficients were determined in this way, the damping coefficients (respectively, κ_3 and κ_4) were adjusted by a similar procedure to fit the amplitude of the real response. However, variations within 20–25% of the values of C_R and C_H did not influence the calculations significantly.

Very good agreement was achieved for all the analysed events using the evaluated sets of constants. Figure 9 shows an example of comparison between the recorded and calculated acceleration at the roof level for the OX-component of the Chibaken-Toho-Oki Earthquake. A notable difference between the maximum value of the recorded and computed acceleration in the time domain was observed only when analysing this event. The reason for this is apparently that the maximum value is very sensitive to the peak, observed at 5 Hz in the recorded data, which could not be simulated adequately.

Effect of the soil non-linearity and the separation of the structure from the soil

It is interesting from a practical point of view how much of the decrease of the soil stiffness and damping coefficients is due to non-linearity and how much to separation. The effect of non-linearity was investigated

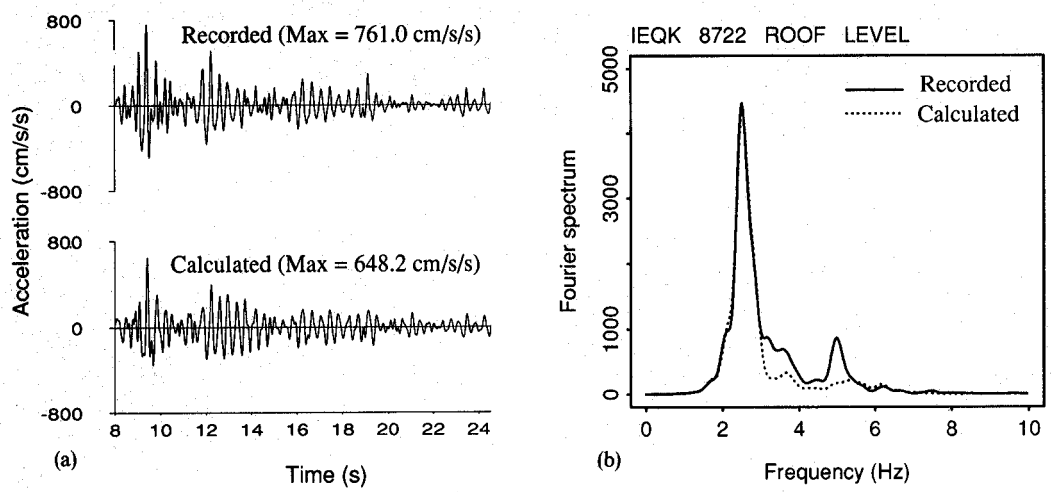

Figure 9. Comparison of recorded and calculated response at the top of the tower: (a) comparison in the time domain; (b) comparison in the frequency domain

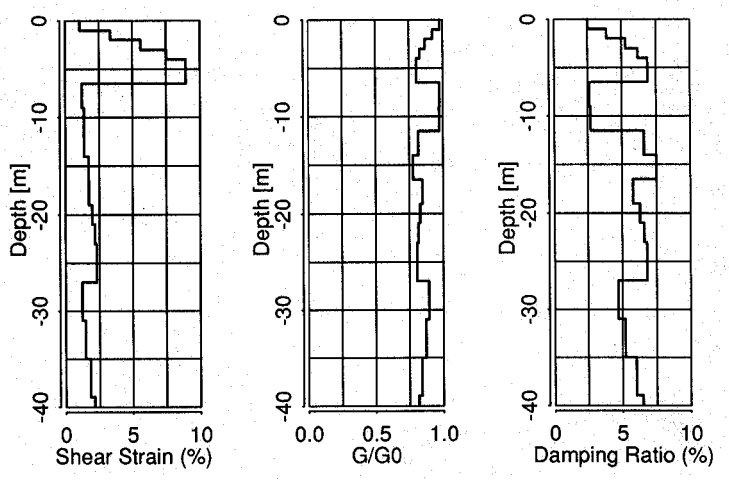

Figure 10. Changes in the shear modulus and damping ratio of the soil (IEQK 8722)

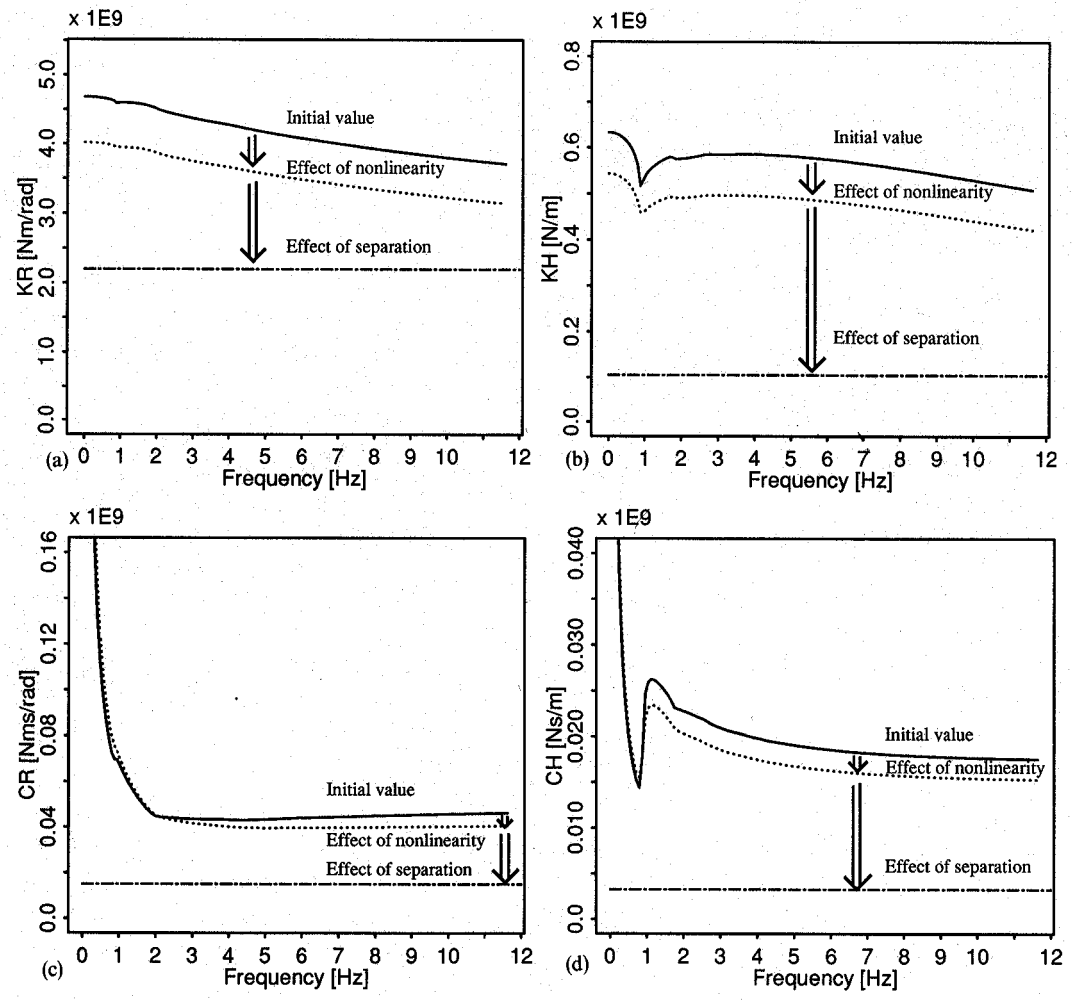

Figure 11. Influence of soil non-linearity and separation of soil from structure on stiffness and damping constants (IEQK 8722, O*Y*-component): (a) change of the rocking spring constant; (b) change of the sway spring constant; (c) change of the rocking dashpot constant; (d) change of the sway dashpot constant

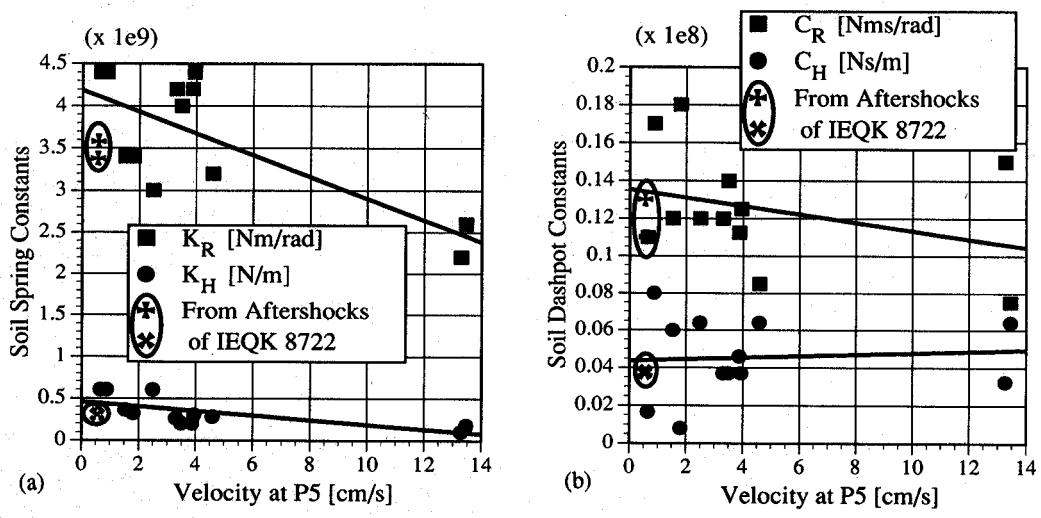

Figure 12. Empirical relation between the peak ground velocity and the soil stiffness and damping constants

with the program SHAKE on the basis of one-dimensional wave propagation theory. Using the earthquake record at P5, the changes in shear modulus and damping ratio were obtained. These changes are visualized in Figure 10. The new values of G and D obtained with SHAKE were substituted in equations (6)–(9) and the stiffness and damping coefficients were recalculated to account for the effect of non-linearity. It should be pointed out, however, that this evaluation is to some extent approximate, because of the assumed one-dimensional wave propagation. Figure 11 shows an example of discrimination between the effect of soil non-linearity and effect of separation on all coefficients for the Chibaken-Toho-Oki Earthquake (IEQK 8722). The lines designating the effect of separation show the equivalent constant values of the coefficients, obtained by the numerical analysis. The separation has a much stronger influence on the weakening of the soil support than the soil non-linearity.

Empirical relationship between the peak ground velocity and the soil parameters

Figure 12 presents graphically empirical relations between the peak ground velocity and the soil constants for 16 earthquake components and corresponding linear curve fits. It can be seen, that generally all the coefficients decrease with the increase of the peak ground velocity, only the sway dashpot coefficient is not strongly affected. Analysis of two weak aftershocks of the Chibaken-Toho-Oki Earthquake (IEQK 8723 and 8726) showed values of the soil constants, which were closer to those, calculated for the preceding strong motion, than for other small earthquakes. This similarity signifies that the soil support remained weaker for a certain period of time after the large event.

CONCLUSIONS

Using recorded earthquake motion of a reinforced concrete tower in Chiba, Japan, effects of soil–structure interaction were investigated. It was found that separation of the soil from the structure occurs under large dynamic loads, leading to redistribution of the stresses from structural weight over the bottom soil. The decreasing of the soil support under large dynamic loads results in a shift of the predominant frequency of the soil–structure system. Using a linear sway-rocking model with constant values of the stiffness and damping coefficients, the behaviour of the soil–structure system was simulated successfully. The influence of the interaction phenomena on the soil parameters was determined by a comprehensive comparative study of recorded and calculated structural response. For each analysed event, a set of best-fitting values of the soil coefficients was determined. A distinct assessment of the effect of soil non-linearity and the effect of

separation on the soil parameters was made. It was found that separation weakens the soil support much more than the soil non-linearity and the soil support remains weaker for a certain period of time after a large earthquake. Simple empirical relationships between the peak ground velocity and the soil spring and dashpot constants for earthquake excitation of different magnitude were found. All the constants decrease with the increase of the peak ground velocity, with the exception of the sway dashpot constant.

REFERENCES

1. M. Novak and Y. Beredugo, 'The effect of embedment on footing vibrations', *Proc. 1st Can. conf. earthquake eng.*, Vancouver, Canada (1971).
2. J. P. Wolf, *Dynamic Soil–Structure Interaction*, Prentice-Hall, Englewood Cliffs, NJ, 1985.
3. A. Mita and J. E. Luco, 'Dynamic response of embedded foundations: a hybrid approach', *Comput. methods appl. mech. eng.* **63**, 233–259 (1987).
4. V. K. Gupta and M. D. Trifunac, 'Seismic response of multistoried buildings including the effects of soil–structure interaction', *Soil dyn. earthquake eng.* **10**, 414–422 (1991).
5. M. I. Todorovska, 'Effect of the depth of embedment on the system response during building–soil interaction', *Soil dyn. earthquake eng.* **11**, 111–123 (1992).
6. EPRI. *Proc.: EPRI/NRC/TPC workshop on seismic soil–structure interaction analysis techniques using data from Lotung, Taiwan*, Palo Alto, California (1987).
7. T. Katayama, F. Yamazaki, S. Nagata, L. Lu and T. Turker, 'A strong motion database for the Chiba seismometer array and its engineering analysis', *Earthquake eng. struct. dyn.* **19**, 1089–1106 (1990).
8. T. Yamagami and Y. Hangai, 'Observations of dynamic soil–structure interaction of reinforced concrete tower', *Bull. earthquake resistant struct. res. center* **19**, 37–45, University of Tokyo (1986).
9. N. Yoshida, T. Yamagami, D. Fujii and Y. Hangai, 'Comparison of analytical results with observation data about soil–structure interaction of a tower', *Proc. symp. comput. methods struct. eng. related fields*, Tokyo, Japan (1986) (in Japanese).
10. M. Hoshiya and K. Ishii, 'Deconvolution method between kinematic interaction and dynamic interaction of soil–foundation systems based on observed data', *Soil dyn. earthquake eng.* **3**, 157–164 (1984).
11. Klaus-Jurgen Bathe and E. Wilson, *Numerical Methods in Finite Element Method*, Prentice-Hall, Englewood Cliffs, NJ, 1976.
12. T. Harada, K. Kubo and T. Katayama, 'Dynamic soil–structure interaction analysis by continuum formulation method', *Report of the Institute of Industrial Science* 29, University of Tokyo (1981).